Miniaturization of Power Dividers by Using Asymmetric CMRC Structures and QWLTs with Low-Cost Materials

Sangwon KITTIWITTAYAPONG [1], Danai TORRUNGRUENG [1], Kittisak PHAEBUA [1], Kitiphon SUKPREECHA [1], Titipong LERTWIRIYAPRAPA [1], Panuwat JANPUGDEE [2]

[1] Research Center of Innovation Digital and Electromagnetic Technology, Dept. of Teacher Training in Electrical Engineering, Faculty of Technical Education, King Mongkut's University of Technology North Bangkok, Bangkok 10800, Thailand
[2] Wireless Network & Future Internet Research Unit, Dept. of Electrical Engineering, Chulalongkorn University, Bangkok, Thailand

sangwon.k@fte.kmutnb.ac.th, dtg@ieee.org, kittisak.p@fte.kmutnb.ac.th, kitiphon7788@gmail.com, titipong.l@fte.kmutnb.ac.th, panuwat.ja@chula.ac.th

Submitted February 29, 2024 / Accepted May 10, 2024 / Online first May 28, 2024

Abstract. *This paper presents the miniaturization of power dividers using asymmetric compact-microstrip-resonant-cell (CMRC) structures employing low-cost materials based on a quarter-wave-like transformer (QWLT). The proposed CMRC-based QWLT power divider is intended for operation at a frequency of 2.4 GHz, utilizing the FR-4 print circuit board (PCB) with a dielectric constant of 4.3 and a substrate thickness of 1.6 mm. The CMRC dimensions include a width of 5.32 mm and a length of 8.52 mm. It is found that a significant 50% size reduction of length is achieved compared to a conventional power divider, while maintaining an insertion loss (IL) of 3.3 dB, as well as achieving the return loss and isolation loss of 20 dB.*

Keywords

Power divider, quarter-wave transformer (QWT), quarter-wave-like transformer (QWLT), compact microstrip resonant cell (CMRC)

1. Introduction

The size of a conventional power divider (PD) depends on an operating frequency [1]. Thus, the traditional PD configuration is cumbersome and unsuited for modern communication systems. A multi-frequency PD has been proposed to enhance the performance of PDs, such as increasing bandwidth and miniaturizing their configuration. In this design, stubs are integrated to broaden the frequency band [2]. In addition, the bandwidth control is achieved through the utilization of diode technology and a DC power source [3]. Futhermore, a coupled line configuration in [4] is incorporated to further enhance the bandwidth. The techniques presented in [2–7] were employed to decrease losses of PDs. However, the physical dimensions of PDs in those prior studies remained unchanged. Various research works have been proposed to address the challenge of reducing the size of PDs.

In [8], an effective miniaturization technique of quarter-wave transformers (QWTs) was proposed based on the quarter-wave-like transformer (QWLT) theory. Note that QWLTs are implemented using multi-section transmission lines (TLs). In addition, multi-section QWLT characteristics are derived analytically and solved via appropriate optimization algorithms for associated TL parameters. It is found that QWLT prototypes yield acceptable return loss without significant bandwidth reduction, comparing to the QWT result.

Previous research works have focused on minimizing the PD size through the utilization of cost-effective FR-4 print circuit boards (PCBs) [9], [10]. In [9], the approach involves the application of multi-section transmission lines for implementing QWLTs in PDs, leading to a significant 25% size reduction compared to that of the traditional PD configuration. An alternative method for size reduction involves the implementation of a compact microstrip resonant cell (CMRC) [11], yielding a total size reduction of 40% in comparison to that of the conventional TL structure [11–14].

Several types of symmetric CMRCs that differing in shape, dimension, and transmission characteristics were proposed. In [15], this proposed configuration facilitates a 33.6% area reduction of PDs. On the other hand, as presented in [16], the miniaturization of PDs exceeds 50% in terms of area. It is noted that, similar to [15], this approach also involves three-element chips. However, installing and soldering the chip elements onto PDs are challenging due to the tiny area allocated for the installed chip elements. In the approach presented in [17], employing an open stub resulted in a size reduction of over 30% for PDs at the frequency of 1.65 GHz. This solution employs a single chip element and a simple structure for fabrication. As reported in [18], the finite defected ground structure (FDGS) achieves a size reduction of 32% for PDs at the frequency of 2.5 GHz. The solution outlined in [19] employs the substrate integrated waveguide (SIW) to decrease the size of PDs, resulting in a size reduction of 10%.

DOI: 10.13164/re.2024.0349

The studies conducted from [16] to [18] demonstrate in the miniaturization of PDs. These solutions exhibit the potential to reduce the PD area ranging from 30% to 52%. In the case of [16], it employs a simple structure with a cost-effective material, incorporating two chip elements in the circuit. Moreover, this solution achieved a smaller size reduction of 33.61% compared to other approaches. The research works in [17] and [18] achieved the PD miniaturization of 32–35% using a single chip element. It is noted that the references [17–19] utilize RT/Duroid and Roger materials, which are relatively expensive. Some previous research works are complicated in the fabrication and installation of chip elements and measurements. In contrast, in terms of a size reduction of conventional PDs, these previous studies achieved a size reduction lower than 40% at the operating frequency. For these reasons, this paper proposes the miniaturization of PDs by employing the QWLT-based PD introduced in [9]. The proposed approach is achieved by modifying the structure from a symmetric CMRC [11] to an asymmetric CMRC configuration in order to further decrease the size of associated TLs for PDs.

The rest of this paper is organized as follows. Section 2 presents brief theories of QWLTs and PDs. In addition, Section 3 shows results and discussions of the proposed CMRC-based QWLT PDs. Finally, conclusions are provided in Sec. 4.

2. Brief Theories of QWLTs and PDs

In this section, the theories of QWLTs and PDs are presented in brief, where the QWLT theory is given first.

2.1 Brief QWLT Theory

In [10], the derivation and properties of QWLTs are presented in details. The theory of QWLTs is briefly summarized below. Figure 1(a) illustrates the QWLT matching circuit, where Z_{in} and Z_L denote the input and load impedances respectively, where Z_{in} and Z_L are real. In addition, Figure 1(b) shows the QWLT model, where Z_0^+ and Z_0^- are the characteristic impedances of the QWLT for the forward and backward propagation directions respectively, and θ_c is the electrical length of the QWLT. Note that $Z_0^{\pm}$ are complex conjugates of each other, which can be readily derived from the associated *ABCD* parameters of actual circuits to implement QWLTs [10], which can be written compactly as

$$Z_0^{\pm} = \frac{\mp 2B}{A - D \mp \mathrm{j}\sqrt{4 - (A+D)^2}} \tag{1}$$

where $Z_0^{\pm}$ can be readily expressed in the polar form as

$$Z_0^{\pm} = \left|Z_0^{\pm}\right| \mathrm{e}^{\mp \mathrm{j}\phi}. \tag{2}$$

Note that $|Z_0^{\pm}|$ and ϕ in (2) are the magnitude and argument of $Z_0^{\pm}$ respectively, and are defined in the following range: $-90° \le \phi \le 90°$. In addition, the effective propagation constant β of the QWLT can be obtained from its *ABCD* parameters as [10]

$$\cos\theta_c = \frac{A+D}{2} \tag{3}$$

where $\theta_c = \beta d$ and d is the physical length of the QWLT. By definition, the slow-wave factor (*SWF*) of the QWLT depends on the wavelength λ_0 of a conventional TL and the wavelength λ of a slow-wave TL structure as follows:

$$SWF = \frac{\lambda}{\lambda_0} \tag{4}$$

where λ can be determined from β defined in (3) as

$$\lambda = \frac{2\pi}{\beta}. \tag{5}$$

Note that a higher SWF results in a more size reduction of TL structures compared to that of the conventional TL.

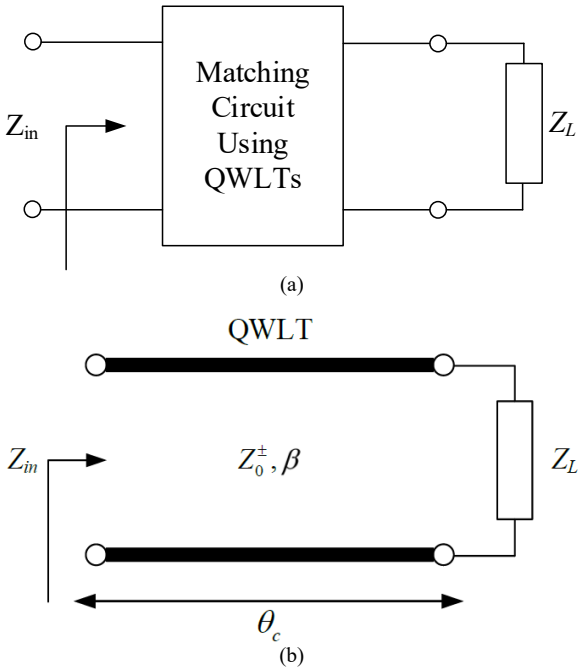

Fig. 1. (a) The QWLT matches an arbitrary real load impedance Z_L to a specific real input impedance Z_{in}. (b) The QWLT model.

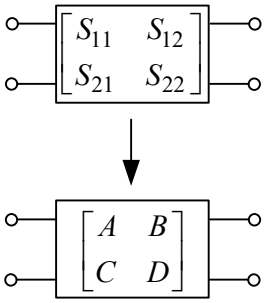

Fig. 2. Conversion of the scattering parameters to the *ABCD*-parameters for the QWLT-parameter calculation.

In [14], it is shown that the electrical length θ_c of the QWLT is given by

$$\theta_c = \begin{cases} \tan^{-1}\left(-\Gamma_{f,L}\cot\phi\right), & \text{when } \begin{matrix} Z_L > Z_{in} \text{ and } \phi < 0, \\ Z_L < Z_{in} \text{ and } \phi > 0 \end{matrix} \text{ or} \\ \tan^{-1}\left(-\Gamma_{f,L}\cot\phi\right)+\pi, & \text{when } \begin{matrix} Z_L > Z_{in} \text{ and } \phi > 0, \\ Z_L < Z_{in} \text{ and } \phi < 0 \end{matrix} \text{ or} \end{cases} \tag{6}$$

where the reflection coefficient $\Gamma_{f,L}$ in (6) is defined as

$$\Gamma_{f,L} = \frac{Z_L - Z_{in}}{Z_L + Z_{in}}. \tag{7}$$

In (7), Z_{in} and Z_L are both real values and given for a specific impedance-matching problem. In addition, it is shown in [14] that $|Z_0^{\pm}|$ can be compactly expressed as

$$\left|Z_0^{\pm}\right| = \sqrt{Z_{in}Z_L}. \tag{8}$$

In this paper, the asymmetric CMRCs are implemented by using asymmetric structures with the required conditions of QWLTs given in (6) to (8), where the *ABCD*-parameters in computing $Z_0^{\pm}$ and β of QWLTs can be obtained from the associated scattering parameters of QWLTs using the standard conversion of two-port parameters as shown in Fig. 2 [1].

To design a QWLT for given Z_{in} and Z_L, it is more convenient to employ the following formulation to obtain valid *ABCD* parameters of actual circuits to implement the desired QWLT, and then compute the QWLT parameters from the known *ABCD* parameters. Note that the relationship between Z_{in} and Z_L in Fig. 1(a) can be written as follows [8]:

$$Z_{in} = \frac{AZ_L + B}{CZ_L + D} \tag{9}$$

where *A, B, C,* and *D* in (9) are the *ABCD*-parameters of the QWLT matching circuit. Using (9) under the condition of reciprocal QWLTs ($AD - BC = 1$) and real Z_{in} results in the following simple relationships [8]:

$$\frac{A}{D} = \frac{Z_{in}}{Z_L}, \tag{10}$$

$$\frac{B}{C} = Z_{in}Z_L. \tag{11}$$

Note that the required conditions in (10) and (11) are more convenient to solve and easy to calculate associated QWLT parameters via (1) and (3).

2.2 Brief Theory of PDs

In this section, the theory of both conventional and CMRC-based QWLT PDs is discussed in brief.

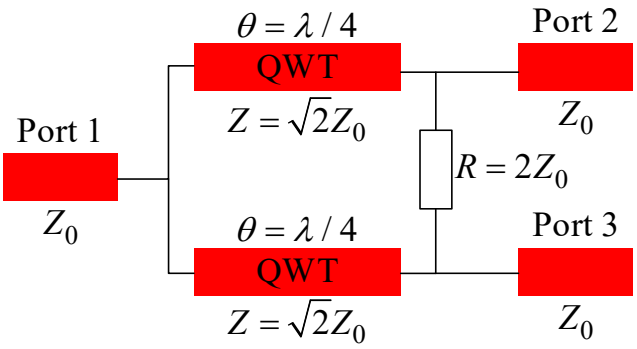

Fig. 3. The schematic diagram of the conventional PD.

2.2.1 Conventional PDs

The conventional PD is designed by using two standard QWTs [1]. Figure 3 shows the schematic diagram of the conventional PD, where λ is the operating wavelength,

$$\theta = \lambda/4, \tag{12}$$

$$Z = \sqrt{2}Z_0, \tag{13}$$

$$R = 2Z_0. \tag{14}$$

Note that θ is the electrical length of QWTs, Z is the characteristic impedance of QWTs, R is the isolation impedance of the conventional PD, and Z_0 is the port impedance. Conventional PDs are simple to design and fabricate; however, their dimensions are determined by the operating wavelength, usually resulting in larger sizes for lower frequencies. In addition, traditional PDs cannot be readily changed in their shape or reduced in size.

2.2.2 CMRC-based QWLT PDs

This subsection shows the concept of CMRC-based QWLT PDs. Figure 4 illustrates the schematic diagram of CMRC-based QWLT PDs, where $Z_0^{\pm}$ are the characteristic impedances of QWLTs, θ_c is their electrical length and $Z_{S,CMRC}$ is the isolation impedance. Note that $Z_0^{\pm}$ and θ_c can be readily determined using the even-odd mode analysis [1], [9] and $Z_{S,CMRC}$ is readily calculated based on the principle outlined in [9]. It should be noted that, with this approach, the CMRC-based QWLT for the even-mode analysis provides that the load impedance $Z_L = 2Z_0$ is matched to the input impedance $Z_{in} = Z_L$. Based on these impedances and a certain value of the argument ϕ defined in (2), the results of minimizing the divider design depending on the QWLT parameters are calculated according to (6) to (8). As pointed out in [9], the *ABCD*-parameters of the QWLT in terms of $Z_0^{\pm}$ and θ_c are useful in the derivation of $Z_{S,CMRC}$ as given below:

$$\begin{bmatrix} A & B \\ C & D \end{bmatrix} = K\begin{bmatrix} Z_0^+ e^{j\theta_c} + Z_0^- e^{-j\theta_c} & Z_0^+ Z_0^- (e^{j\theta_c} - e^{-j\theta_c}) \\ e^{j\theta_c} - e^{-j\theta_c} & Z_0^- e^{j\theta_c} + Z_0^+ e^{-j\theta_c} \end{bmatrix}, \tag{15}$$

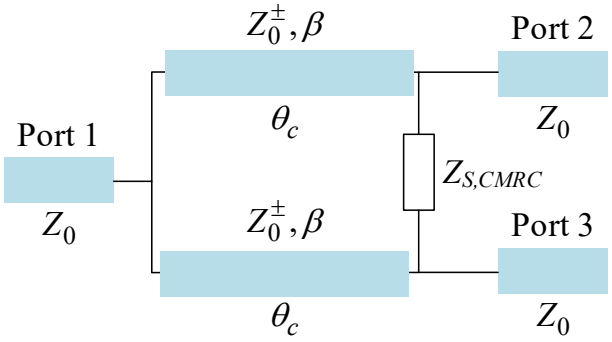

Fig. 4. The schematic diagram of the CMRC-based QWLT PDs.

$$K = \frac{1}{Z_0^+ + Z_0^-}. \tag{16}$$

In the next section, associated results of both conventional and CMRC-based QWLT PDs are provided. In addition, comparisons and discussions are also given.

3. Results and Discussions

The core concept of this paper involves modifying a symmetric CMRC to an asymmetric CMRC through an application of QWLTs. Figures 5 and 6 illustrate the symmetric and asymmetric CMRC structures, respectively. The goal of this study is to achieve a 50% size reduction at the operating frequency of 2.4 GHz. Note that the prototype of the proposed CMRC-based QWLT PD is shown in Fig. 7(b), where its structure is compact and simple for implementation. The conventional and proposed PDs are designed on a lossless FR-4 substrate material with a dielectric constant of 4.2 and a thickness of 1.6 mm. The conductor is assumed to be a perfect electric conductor (PEC) to ensure lossless TL characteristics. This study compares the performance of the two PDs at 2.4 GHz. Note that the isolation resistance R_s in Fig. 7(a) for the conventional Wilkinson PD is obtained as shown in [1], while the isolation impedance $Z_{S,CMRC}$ in Fig. 7(b) for the proposed CMRC-based QWLT PD is designed according to [9].

The conventional Wilkinson PD is shown in Fig. 7(a), where the length of each TL is equal to $\lambda/4$ (QWT) and the

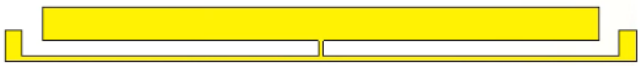

Fig. 5. A symmetric CMRC structure [11].

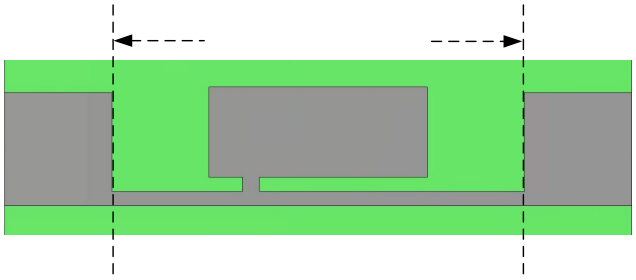

Fig. 6. An asymmetric CMRC structure modified from the structure in Fig. 5.

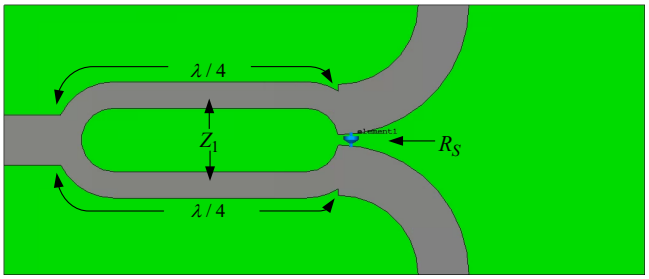

(a)

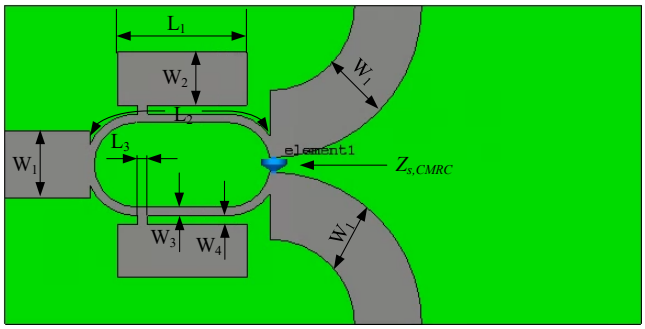

(b)

Fig. 7. (a) Conventional Wilkinson PD. (b) The proposed CMRC-based QWLT PD.

Parameter	Dimension (mm)
W_1	3.16
W_2	2.51
W_3	0.40
W_4	0.40
L_1	6.08
L_2	11.48
L_3	0.48

Tab. 1. Dimensions of the CMRC-based QWLT PD.

isolation impedance R_S is given in (14). In addition, the characteristic impedance Z_1 of two QWTs is provided in (13). Note that $\lambda/4$ is equal to 22.96 mm at 2.4 GHz in Fig. 7(a) and the length L_2 of the proposed CMRC-based QWLT PD is equal to 11.48 mm in Fig. 7(b). The QWLT based on an asymmetric CMRC structure in Fig. 7(b) can be found using the even-mode analysis as detailed in [1]; i.e., the QWLT transforms the load impedance of $2Z_0$ to the input impedance of Z_0, where Z_{in} and Z_L in (10) and (11) in this case are equal to Z_0 and $2Z_0$, respectively. Note that the *ABCD* parameters in (10) and (11) are determined numerically by simulation of the proposed asymmetric CMRC structure in Fig. 6 using the CST-MW Studio [20] for desired characteristics. By solving (10) and (11) simultaneously to obtain the *ABCD* parameters, each optimized asymmetric CMRC structure is shown in Fig. 7(b), where its parameters are given in Tab. 1. Once the *ABCD* parameters are known, the QWLT parameters can be computed using (1) to (3) and each QWT of the conventional Wilkinson PD can be replaced by the QWLT as shown in Fig. 7(b) [11].

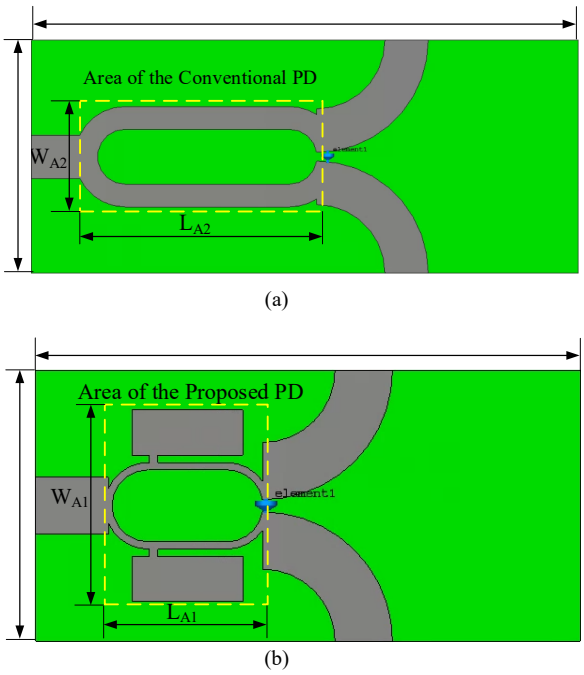

Fig. 8. The circuit area and dimension of (a) the conventional Wilkinson PD and (b) the proposed CMRC-based QWLT PD.

In [9], after straightforward manipulation, $Z_{S,CMRC}$ can be expressed compactly as

$$Z_{S,CMRC} = 2Z_0 \frac{\sin^2 \theta_c}{\cos^2 \phi} - j\sqrt{2}Z_0 \frac{\sin 2\theta_c}{\cos \phi} \qquad (17)$$

where θ_c of each QWLT is equal to 69.26° (using (6)), ϕ of each QWLT in Fig. 7(b) and using Tab. 1 is chosen to be 7.2° [9], and $|Z_0^{\pm}| = 70.71\ \Omega$ (using (8) with $Z_{in} = Z_0$ and $Z_L = 2Z_0$). Using (17), it is found that $Z_{S,CMRC}$ is equal to (88.86 – j47.20) Ω, which can be implemented using the resistor of 88.70 Ω and the capacitor of 1.45 pF at 2.4 GHz.

Figures 8(a) and 8(b) show the circuit dimension of the conventional Wilkinson PD and the proposed CMRC-based QWLT PD. In addition, Table 2 presents a comparison of the circuit dimension between two PDs. It is found that the total area of the conventional Wilkinson PD in Fig. 8(a) is equal to 679.20 mm², while that of the proposed CMRC-based QWLT PD in Fig. 8(b) is equal to 450.30 mm². In addition, the PD areas of the conventional Wilkinson PD and proposed CMRC-based QWLT PD as shown in Fig. 8 are equal to 126.87 mm² and 90.35 mm², respectively. Thus, it is obvious that both areas of the proposed PD are significantly smaller than those of the conventional one.

Table 3 shows the QWLT parameters of the asymmetric CMRC structure in Fig. 7(b), computed using (1) to (8) by the *ABCD*-parameters obtained as a result of converting the optimized scattering parameters. The magnitudes of characteristic impedances $|Z_0^+|$ and $|Z_0^-|$ are equal to 77.62 Ω and 77.64 Ω respectively, which are slightly different. In addition, their phases, ϕ^+ and ϕ^-, are equal to –8.65° and 8.60°, respectively. Note that Z_0^+ and Z_0^- are almost complex conjugate of each other as expected.

Parameter	Dimension (mm)
L_{S1}	30
L_{S2}	40
L_{A1}	8.52
L_{A2}	17.38
W_{S1}	15.01
W_{S2}	16.98
W_{A1}	10.63
W_{A2}	7.30

Tab. 2. Dimension comparison between the conventional Wilkinson PD and the proposed CMRC-based QWLT PD.

QWLT parameter	Value
$\lvert Z_0^+ \rvert$	77.62 Ω
$\lvert Z_0^- \rvert$	77.64 Ω
ϕ^+	–8.65°
ϕ^-	8.60°
SWF	3.66

Tab. 3. The QWLT parameters of the asymmetric CMRC structure in Fig. 7(b) using Tab. 1.

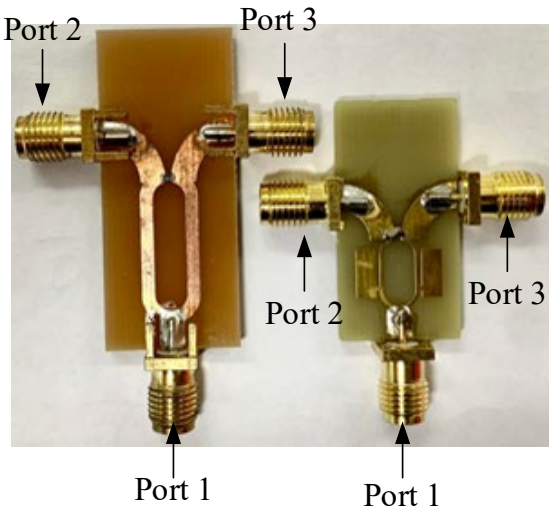

Fig. 9. The fabricated prototypes of the conventional Wilkinson PD (left) and the proposed CMRC-based QWLT PD (right).

Figure 9 shows the fabricated prototypes of the conventional Wilkinson PD and the proposed CMRC-based QWLT PD. From Fig. 9, the size comparison reveals that the PD length of the latter is about 50% of that of the former, where the latter provides a significant size reduction indeed.

Figure 10 illustrates the simulated and measured frequency responses of the CMRC-based QWLT PD compared to those of the conventional Wilkinson PD. Note that Port 1 is the input port, while Ports 2 and 3 represent the output

ports. Note that Figure 10(a) shows the magnitude of S_{11} ($|S_{11}|$), while Figure 10(b) illustrates the isolation results ($|S_{23}|$). It is found that $|S_{11}|$ and $|S_{23}|$ are below –25 dB and –20 dB at 2.4 GHz, respectively. It is found that the simulated and measured results are in good agreement. However, there is a slight discrepancy in resonant frequencies between the measured and simulated results for both conventional and CMRC-based QWLT PDs. In addition, Figure 11 shows a comparison of $|S_{21}|$ and $|S_{31}|$ of simulated and measured results for both conventional and CMRC-based QWLT PDs. It is found that the slight discrepancy in magnitude of about 0.5 dB at 2.4 GHz between simulated and measured results is obtained.

In addition, Table 4 compares the proposed CMRC-based QWLT PD with other PDs selected from previous research works, emphasizing key parameters such as the length reduction, the number of chip elements used, the substrate material, the operating frequency, the circuit size, and the S-parameters given at the lowest frequency for each reference. Note that the PDs in [2–7] did not achieve any size reduction. Furthermore, PDs in [3], [6], and [7] utilized both resistor and capacitor chips, leading to complex structures. In [9] and [15–19], the size reduction of PDs can be achieved as shown in Tab. 4. Note that the PD in [16] incorporated more than two chip elements in the circuit, and the PD in [19] has no chip element but its size reduction is lower than 20%.

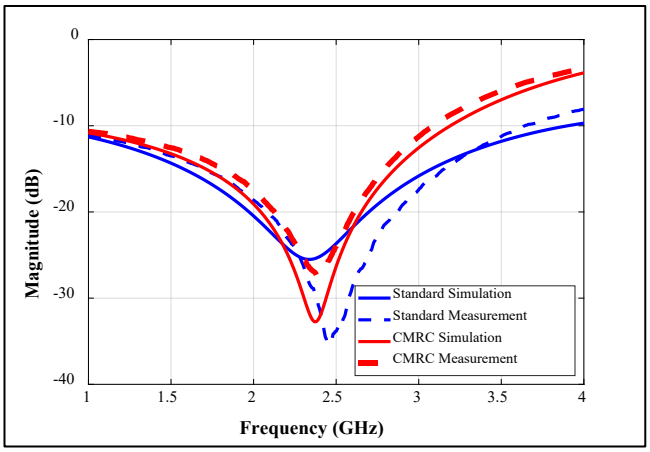

(a)

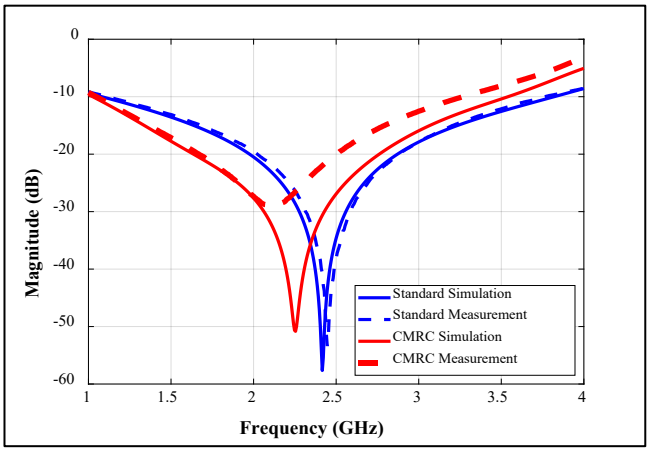

(b)

Fig. 10. Simulated and measured frequency responses of the conventional Wilkinson PD and the CMRC-based QWLT PD: (a) $|S_{11}|$, (b) $|S_{23}|$.

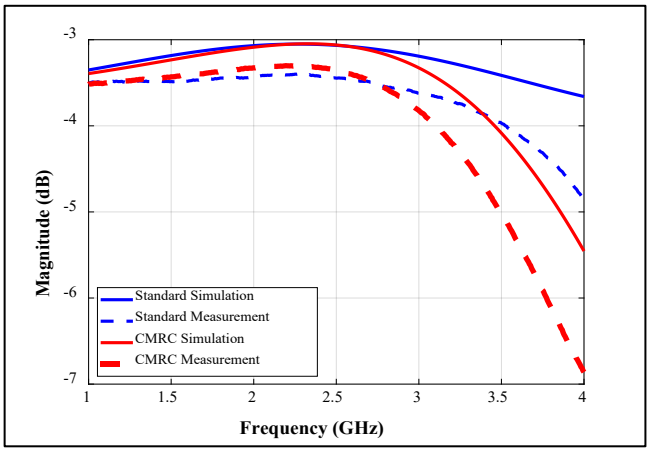

(a)

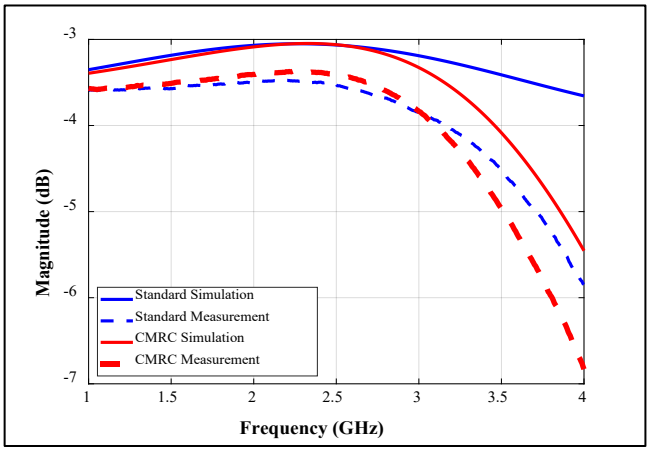

(b)

Fig. 11. Simulated and measured insertion losses of the conventional Wilkinson PD and the CMRC-based QWLT PD: (a) $|S_{21}|$, (b) $|S_{31}|$.

To demonstrate the flexibility in controlling the passband by adjusting the center frequency, the total length of the CMRC-based QWLT PD (L_{A1}) and the total length of the conventional Wilkinson PD (L_{A2}) defined in Fig. 8 are varied to see their effects on the frequency responses of $|S_{11}|$, $|S_{21}|$, $|S_{31}|$ and $|S_{23}|$ as shown in Fig. 12. In this paper, both PDs are designed at 2.4 GHz, where L_{A1} and L_{A2} are equal to 8.52 and 17.38 mm (the designed values) as shown in Tab. 2, respectively. It is found that as L_{A1} and L_{A2} are decreased from the designed values, the center frequency is shifted towards the higher frequency and vice versa as expected. Thus, the CMRC-based QWLT PD is flexible to control the passband by adjusting the center frequency indeed. Finally, it should be pointed out that the described approach in this paper can be applied to systematically design similar power dividers and other microwave circuits if they possess the quarter-wave transformers (QWTs) in their circuits by replacing the QWTs by the corresponding QWLTs based on asymmetric CMRC structures. Note that the QWLTs can be systematically designed by using the brief design procedure outlined in Sec. 3 (see the description of Fig. 7(b)).

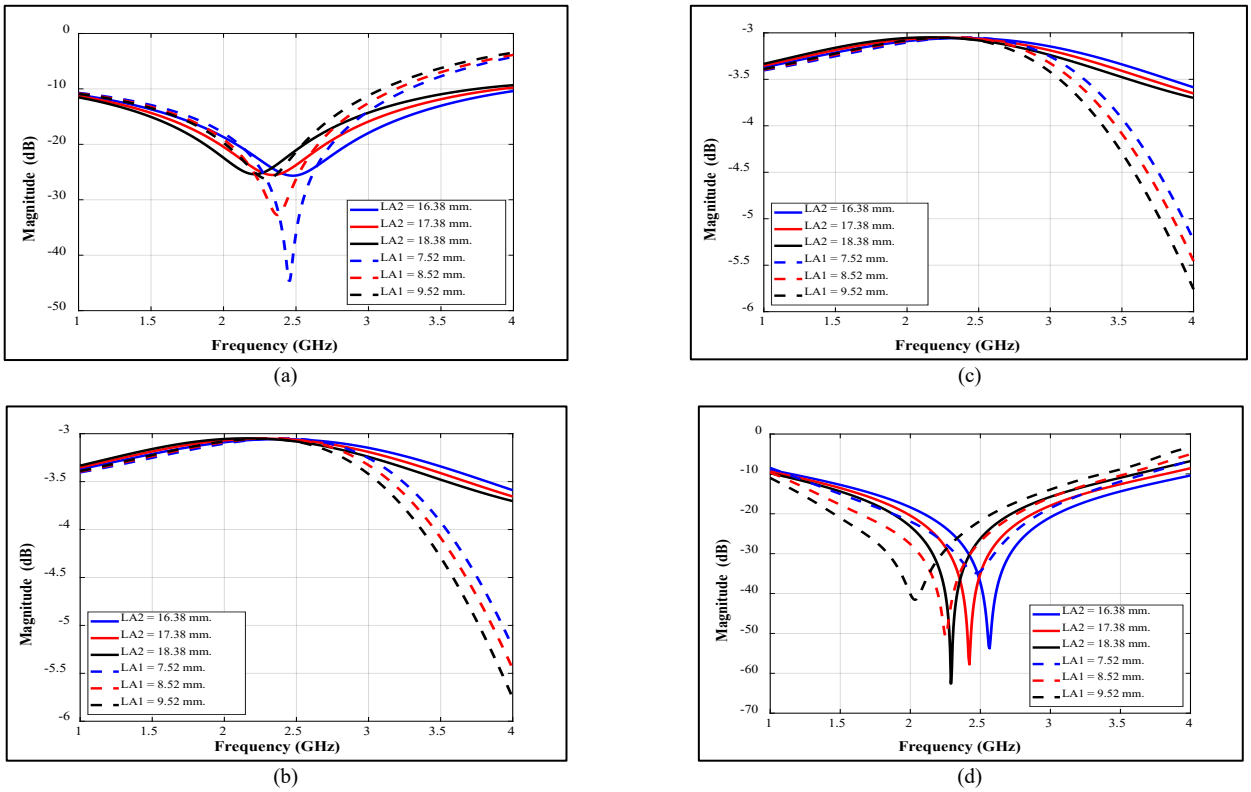

Fig. 12. Effects of L_{A1} and L_{A2} to the frequency responses of the CMRC-based QWLT PD and the conventional Wilkinson PD, respectively: (a) $|S_{11}|$, (b) $|S_{21}|$, (c) $|S_{31}|$, (d) $|S_{23}|$.

Ref.	Substrate material	Number of chip elements	Length reduction compared with $\lambda_g/4$ (%)	Operating frequency (GHz)	Circuit size ($\lambda_g \times \lambda_g$)	$\|S_{11}\|$, $\|S_{21}\|$, $\|S_{31}\|$, $\|S_{23}\|$ (dB)
[2]	RO4350B	0	0	2.0, 4.4 and 5.0	2.15 × 2.15	–20.00, –4.44, –3.10, –7.39
[3]	RO4350B	11	0	2.4	2.03 × 1.37	–20.00, –1.12, –14.90, –13.70
[4]	RT/Duroid 5880	1	0	1.0-7.0	1.96 × 2.09	–36.00, –3.24, –3.24, –29.00
[5]	RT/Duroid 5880	0	0	14.5	2.55 × 1.68	–33.00, –3.20, –3.20, –22.00
[6]	FR-4	9	0	3.5	3.41 × 2.56	–25.00, –3.00, –3.00, –52.00
[7]	Material (dielectric constant of 2.94)	1,5 and 8	0	10.5	2.11 × 2.11	–21.00, –3.30, –3.30, –20.00
[9]	FR-4	2	25	2.4	0.77 × 0.74	–22.00, –3.60, –3.60, –30.00
[15]	FR-4	2	0	2.4	1.74 × 1.51	–26.73, –3.67, none, none
[16]	Roger 4003C	3	0	2.4, 5.9	0.73 × 0.73	–26.10, –3.05, –3.30, –28.00
[17]	RT/Duroid 5880	1	28.76	1.65	0.71 × 0.47	–31.00, –3.04*, –3.04*, –43.00
[18]	RT/Duroid 5880	1	31.73	2.75	1.80 × 0.63	–31.00, –8.00 –10.00, –35.00
[19]	RT/Duroid 5870	0	10.71	3.47, 4.73 and 6.31	0.12 × 0.24	–27.89, –4.16, –3.88, –11.20
This work	FR-4	2	35.21	2.4	0.48 × 0.60	–25.00, –3.40, –3.47, –40.10

λ_g is the guided wavelength of the substrate material.
The S-parameters are given at the lowest frequency for each reference, and the superscript * denotes the results obtained from simulations.

Tab. 4. Comparison of key parameters of the proposed CMRC-based QWLT PD and selected PDs in previous research works.

4. Conclusions

In this paper, a novel PD is miniaturized using asymmetric CMRC structures with low-cost materials based on QWLTs. The results showcase a remarkable miniaturization of 35.21% compared with $\lambda_g/4$ and approximately 50% compared to the length of the conventional PD at 2.4 GHz, while maintaining good performance. Comparisons between simulated and measured results demonstrate good agreement, with the isolation $|S_{23}|$ and magnitude of reflection coefficient $|S_{11}|$ below 20 dB. The insertion loss $|S_{21}|$ and $|S_{31}|$ are at 3.3 dB. In addition, the proposed PD model is simple and straightforward to fabricate. In the future, the research will explore other asymmetric CMRC structures for additional size reduction of various microwave devices.

Acknowledgments

This research was funded by King Mongkut's University of Technology North Bangkok, Contract no. KMUTNB-PHD-62-08 and KMUTNB-67-KNOW-03.

References

[1] POZAR, D. M. *Microwave Engineering*. 4th ed. New Jersey: John Wiley & Sons, 2012. ISBN: 0-471-67751-X

[2] YANG, Y., HU, N., XIE, W., et al. A compact tri-band impedance-transforming power divider with independent controllable power division ratios and enhanced bandwidths. *IEEE Access,* 2019, vol. 7, p. 25185–25194. DOI: 10.1109/ACCESS.2019.2900060

[3] ILYAS, S., SHOAIB, N., NIKOLAOU, S., et al. A wideband tunable power divider for SWIPT systems. *IEEE Access,* 2020, vol. 8, p. 30675–30681. DOI: 10.1109/ACCESS.2020.2970781

[4] MAKTOOMI, M. H., BANERJEE, D., HASHMI, M. S. An enhanced frequency-ratio coupled-line dual-frequency Wilkinson power divider. *IEEE Transactions on Circuits and Systems-II: Express Briefs*, 2018, vol. 65, no. 7, p. 888–892. DOI: 10.1109/TCSII.2017.2749407

[5] DANG, Z., ZHANG, Y., ZHU, H. L., et al. An isolated out-of-phased 3-dB power divider via wavegude-to-microstrip transition. *IEEE Microwave and Wireless Components Letters*, 2022. vol. 32, no. 1, p. 21–24. DOI: 10.1109/LMWC.2021.3114413

[6] PIACIBELLO, A., PIROLA, M., GHIONE, G. Generalized symmetrical 3 dB power dividers with complex termination impedances. *IEEE Access*, 2020. vol. 8, p. 38239–38247. DOI: 10.1109/ACCESS.2020.2976153

[7] MOULAY, A., DJERAFI, T. Wilkinson power divider with fixed width substrate-integrated waveguide line and a distributed isolation resistance. *IEEE Microwave and Wireless Components Letters*, 2018, vol. 28, no. 2, p. 114–116. DOI: 10.1109/LMWC.2018.2790706

[8] SATITCHANTRAKUL, T., CHUDPOOTI, N., AKKARAEK-THALIN, P., et al. An implementation of compact quarter-wave-like-transformers using multi-section transmission lines. *Radioengineering,* 2018, vol. 27, no. 1, p. 101–109. DOI: 10.13164/re.2018.0101

[9] KORANANAN, S., JANPUGDEE, P., TORRUNGRUENG, D. Miniaturization of power dividers using quarter-wave-like transformers (QWLTs). In *International Symposium in Antennas and Propagation (ISAP)*. Phuket (Thailand), 2017, p. 1–2. DOI: 10.1109/ISANP.2017.8228878

[10] TORRUNGRUENG, D. *Advanced Transmission-Line Modeling in Electromagnetics*. 1st ed. Charansanitwong Printing, 2012. ISBN: 978-616-305-017-5

[11] KURGAN, P., FILIPCEWICZ, J., KITLINSKI, M. Development of compact microstrip resonant cell aimed at efficient microwave component size reduction. *IET Microwave, Antennas & Propagation*, 2012, vol. 6, no. 12, p. 1291–1298. DOI: 10.1049/iet-map.2012.0192

[12] KITTIWITTAYAPONG, S., SATITCHANTRAKUL, T., TORRUNGRUENG, D., et al. Miniaturized low-loss impedance transformers using bi-characteristic impedance transmission lines (BCITLs). In *The 9th International Electrical Engineering Congress (iEECON)*. Pattaya (Thailand), 2021, p. 595–598. DOI: 10.1109/iEECON51072.2021.9440240

[13] KITTIWITTAYAPONG, S., SATITCHANTRAKUL, T., TORRUNGRUENG, D., et al. Design of miniaturized impedance transformers using quarter-wave-like transformers implemented by asymmetric compact microstrip resonant cells. In *The 9ith International Electrical Engineering Congress (iEECON)*. Pattaya (Thailand) 2021, p. 607–610. DOI: 10.1109/iEECON51072.2021.9440254

[14] JONGSUEBCHOKE, I., AKKARAEKTHALIN, P., TORRUNGRUENG, D. Theory and design of quarter-wave-like-transformer implemented using conjugately characteristic-impedanced transmission lines. *Microwave and Optical Technology Letters*, 2016, vol. 58, no. 11, p. 2614–2619. DOI: 10.1002/mop.30120

[15] MAHOUTI, P., BELEN, M. A., PARTAL, H. P., et al. Miniaturization with dumbbell shaped defected ground structure for power divider designs using Sonnet. In *International Review of Progress in Applied Computational Electromagnetics (ACES)*. Williamsburg (VA, USA), 2015, p. 1–2. ISBN: 978-0-9960-0781-8

[16] BARZDENES, V., VASJANOV, A., GRAZULEVICIUS, G., et al. Design and miniaturization of dual-band Wilkinson power dividers. *Journal of Electrical Engineering,* 2020, vol. 71, no. 6, p. 423–427. DOI: 10.2478/jee-2020-0058

[17] HAYATI, M., ROSHANI, S. A novel Wilkinson power divider using open stubs for the suppression of harmonics. *The Applied Computational Electromagnetics Society Journal (ACES)*, 2013, vol. 28, no. 6, p. 501–506. ISSN: 1943-5711 (online)

[18] ROSHANI, S., SIAHKAMARI, P. Design of a compact 1:2 and 1:4 power divider with harmonic suppression using resonator. *Wireless Personal Communications*, 2022, vol. 126, no. 3, p. 2635–2645. DOI: 10.1007/s11277-022-09833-5

[19] PRADHAN N. C., SUBRAMANIAN, K. S., BARIK, R. K., et al. Design of compact substrate integrated waveguide based triple-and quad-band power dividers. *Microwave and Wireless Components Letters*, 2021, vol. 31, no. 4, p. 365–368. DOI: 10.1109/LMWC.2021.3061693

[20] *CST-MW Studio*, Comput. Simul. Technol., Framingham, MA, USA, 2017.

About the Authors …

Sangwon KITTIWITTAYAPONG received a bachelor degree of technical education (2014) in Electrical Engineering, master degree of technical education (2019) in Telecommunications Engineering, and studying doctor degree Faculty of Technical Education since 2019 in Electrical Engineering education from King Mongkut's University of

Technology North, Bangkok, Thailand. In 2023, he is a lecturer in the Faculty of Technical Education, Dept. of Teacher Training in Electrical Engineering Education, King Mongkut's University of Technology North Bangkok, Thailand.

Danai TORRUNGRUENG (corresponding author) received his B.Eng. degree in Electrical Engineering (EE) from Chulalongkorn University, Bangkok, Thailand, in 1993. He obtained his M.S. and Ph.D. degrees in EE from The Ohio State University in 1996 and 2000, respectively. From 1995 to 2000, he was a Graduate Research Assistant (GRA) in the Department of Electrical Engineering, ElectroScience Laboratory of The Ohio State University. From 2002 to 2017, he worked in the Electrical and Electronic Engineering Department in the Faculty of Engineering and Technology, Asian University, Chonburi, Thailand. At present, he is a Professor in the Department of Teacher Training in Electrical Engineering in the Faculty of Technical Education, King Mongkut's University of Technology North Bangkok, Bangkok, Thailand.

In 2000, he won an award in the National URSI Student Paper competition at the 2000 National Radio Science Meeting in Boulder, Colorado. From 2004 to 2009, he invented generalized Smith charts, called T-charts or meta-Smith charts, to solve several problems associated with conjugately characteristic-impedance transmission lines (CCITLs) and bi-characteristic-impedance transmission lines (BCITLs), including their useful applications in applied electromagnetics. He authored Meta-Smith Charts and Their Potential Applications (Morgan & Claypool, 2010) and Advanced Transmission-Line Modeling in Electromagnetics (Charansanitwong Printing, 2012). His research interests are electromagnetic sensors, fast computational electromagnetics, rough surface scattering, propagation modeling, electromagnetic wave theory, microwave theory, and techniques and antennas. He is currently a senior member of the IEEE, and a member of the ECTI, where he served as an ECTI technical chair in electromagnetics from 2014 to 2017. In addition, he served as a TPC co-chair of TJMW2016, a vice co-chair of TJMW2017, and the TPC chair of ISAP2017. Furthermore, he is a co-founder of the Innovative Electromagnetics Academy of Thailand (iEMAT), founded in 2013.

Kittisak PHAEBUA received the B.Eng. and M.Eng. degrees in Telecommunication Engineering and the Ph.D. (Eng.) degree in Electrical Engineering from the King Mongkut's Institute of Technology Ladkrabang (KMITL), Bangkok, Thailand, in 2006, 2008, and 2012, respectively. He is currently an Assistant Professor with the Department of Teacher Training in Electrical Engineering, at King Mongkut's University of Technology North Bangkok, Thailand. His research interests include the computation of electromagnetic using high-frequency techniques and antenna and microwave filter design for wireless communication systems.

Kitiphon SUKPREECHA received a bachelor's degree of Technical Education (2021) in Electrical Engineering, master's degree of technical education (2023) in Telecommunications Engineering and since 2023 has been studying doctor degree Faculty of Technical Education in Electrical Engineering Education, King Mongkut's University of Technology North, Bangkok, Thailand.

Titipong LERTWIRIYAPRAPA received the B.S.Tech.Ed. degree in Electrical Engineering from the King Mongkut's University of Technology North Bangkok, in 1996, the M.Eng. degree in Electrical Engineering from the King Mongkut's Institute of Technology Ladkrabang, in 2000, and the M.Sc. and Ph.D. degrees in Electrical Engineering from The Ohio State University, Columbus, OH, USA, in 2006 and 2007, respectively. He is currently an Associate Professor with the Department of Teacher Training in Electrical Engineering, King Mongkut's University of Technology North Bangkok. His research interests include electromagnetic theory, metamaterial, asymptotic, computational electromagnetics, and hybrid methods. He has received the Third Place in the 2007 USNC/CNC URSI Student Paper Competition, held in Ottawa, Canada, and the Best Paper Award in the 2008 International Symposium on Antennas and Propagation (ISAP2008), held in Taiwan. He serves as a board of the ECTI Association, from 2012 to 2015 and from 2020 to 2023.

Panuwat JANPUGDEE received the B.E. degree (Hons.) in Electrical Engineering from Chulalongkorn University, Thailand, and the M.S. and Ph.D. degrees in Electrical Engineering from The Ohio State University, USA. He is currently an Assistant Professor with the Department of Electrical Engineering, Chulalongkorn University. He has extensive experience in the uniform geometrical theory of diffraction (UTD) and its applications to radiation and scattering problems. His research interests include antennas, computational electromagnetics, and microwave engineering. He has also had some experience in the industry. He is a Founding Member of the Innovative Electromagnetic Academic of Thailand (iEMAT). He was the Vice Chair of the IEEE MTT/AP/ED Joint Chapter, Thailand Section. He has been a Reviewer of IEEE Transactions on Antennas and Propagation, IEEE Antennas and Wireless Propagation Letters, and IET Microwave, Antennas and Propagation.